https://doi.org/10.5194/sp-2022-3
Preprint. Discussion started: 23 September 2022

STATE OF THE PLANET Discussions

Ocean Heat Content in the Iberian-Biscay-Ireland regional seas

Álvaro de Pascual-Collar[1], Roland Aznar[1], Bruno Levier[2], Marcos García-Sotillo[1]

[1]Nologin Consulting, Avda. de Ranillas 1D, 50018 Zaragoza, España.
[2]Mercator Ocean, 8-10, rue Hermès, 31520, Ramonville Saint-Agne, France

Correspondence to: Álvaro de Pascual-Collar (alvarodepascual@nologin.es)

Abstract.

The ocean has the largest heat capacity of any single component of the climate system and plays a key dominant role in global heat content changes. Several recent studies have found that the Ocean Heat Content (OHC) has increased during the last decades, not only at a global scale, but also at regional/basin scales.

To analyse OHC variability in the Iberia-Biscay-Ireland (IBI) region, several Copernicus Marine model and observed derived products are used together to provide multi-product estimations of OHC anomalies over the water column (at layers upper 150 m, 700 m, and 2000 m). This work provides an exhaustive analysis of spatial and temporal variability of OHC in the Northeast Atlantic region providing an analysis of area-averaged time series, trend maps, and trends linked with the main water masses found in the IBI region.

The analysis of trends reveals that, despite a significant warming of the region in the period 1993-2020 (at rates of 0.4 W/m^2), the thermohaline variability of subsurface water masses mainly dominates the OHC variability over the upper 2000 m. Additionally, vertical profiles of OHC trends are investigated, linking them with the vertical distribution of water masses; and describing how coupled inter-annual variability of Sub-Artic Intermediate Water, Mediterranean Outflow Water, and Labrador Sea Water accounts for an important part of the total OHC variability in the region.

Short summary.

The article comprises an exhaustive analysis of the Ocean Heat Content in the Northeast Atlantic region. The variability of Ocean Heat Content is studied, and results are linked with the variability of the main water masses found in the region. Results show how the coupled inter-annual variability of water masses accounts for an important part of the total Ocean Heat Content variability in the region.

1. Introduction

It is well established that the main storage (>90%) of extra heat from increasing greenhouse gasses is absorbed by the oceans; consequently, oceans are the dominant source of changes in global warming (Levitus et al., 2005; Levitus et al. 2012; Trenberth et al. 2014; Cheng et al. 2017; von Schuckmann et al. 2020; Gulev et al. 2021). Additionally, the heat stored in oceans has increased during the last decades not only at global scale, but also at basin scales (Gulev et al., 2021; Abraham et al., 2013).

https://doi.org/10.5194/sp-2022-3
Preprint. Discussion started: 23 September 2022

Therefore, Ocean Heat Content (OHC) is one of the six Global Climate Indicators recommended by the World Meteorological Organisation for Sustainable Development Goal 13 implementation (WMO, 2017).

Ideally, the estimations of OHC are integrated over the full depth of the ocean, but for limitations related to the observing system, this is typically done from ocean's surface down to a reduced depth (such as 700 m or 2000 m). These levels are because, before year 2000, temperature measurements were most often taken in the upper 700 m of the water column, but by about 2005 the Argo array had sufficient space-time sampling to yield an improved measure of OHC down to a depth of 2000 m (von Schuckmann et al., 2016; Abraham et al., 2013; Cheng et al., 2022; Cheng et al., 2017).

One of the Copernicus Marine service products are the Ocean Monitoring Indicators (OMIs) which are free downloadable trends and data sets covering the past quarter of a century. These are indicators that allow us to track the vital health signs of the ocean and changes in line with climate change. Among the multiple OMIs provided by Copernicus Marine, an important family are the indicators focused on evaluating OHC trends and variability. Particularly, the indicator GLOBAL_OMI_OHC_trend (see Table 1 for more details on the product; hereafter this product will be referred as GLO-OMI-trend) provides a global map of trends of OHC integrated in the upper 2000 m. Attending to the spatial variability of trends in the IBI region, this global OMI shows spatial variability of trends, ranging from negative trends of -5 W/m^2 northward of the parallel 40º N, up to positive trends of 2.5 W/m^2 observed westward of the Gulf of Cadiz. However, this global info should be treated cautiously when looking at regions closed to coastal areas and marked by the combination of on-shelf and open waters, such as it occurs in the IBI domain. Indeed, availability of higher resolution specific regional products allows us to refine the study of OHC trends in this IBI region.

Previous works presented in Copernicus Marine OSRs detected warmings of 0.9 ± 0.4 W/m^2 in the upper 700 m in the IBI region. These studies concluded that the positive Earth's energy imbalance dominates the observed regional changes around Europe, but the year-to-year variability in the region potentially masks the long-term warming trend (von Schuckmann et al., 2016; von Schuckmann et al., 2018). However, and despite the area-averaged OHC trends show the same ranges that the global trends, the analysis of specific water masses suggest specific behaviours. For example, Potter and Lozzier (2004), based on fifty years of hydrographic data, studied the temperature and salinity trends of the Mediterranean Outflow Water (MOW), finding positive trends that lead to a heat content gain in the MOW reservoir that overpasses the average gain of the North Atlantic basin. Hence, the analysis of the heat stored by the diverse water masses in the IBI region may provide information about the OHC trends at regional and local scales. Although the literature on OHC variability of specific water masses in the IBI region is rather limited; nevertheless, several studies have concentrated efforts to assess the thermohaline variability of the water masses, these studies give some clues about what can be expected regarding the OHC.

The distribution of diverse water masses is one of the main sources of variability (spatial and temporal) in the IBI region. In this region, literature describes a number of water masses but three groups of salinity extrema mainly determine the intermediate hydrographic structure: a subsurface salinity minima connected with Sub-Artic Intermediate Water (SAIW) at potential density anomalies $27.3 < \sigma_\theta$ kg/m3, salinity maxima connected with Mediterranean Outflow Water (MOW) at the neutral density $27.25 < \sigma_\theta < 27.45$ kg/m3, and salinity minima connected with Labrador Sea Water (LSW) underneath the

https://doi.org/10.5194/sp-2022-3
Preprint. Discussion started: 23 September 2022

isopycnal 27.8 > σ_θ kg/m3 (Talley and McCarney, 1982; Iorga and Lozier, 1999(a); Iorga and Lozier, 1999(b); van Aken, 2000; Prieto et al., 2013; de Pascual-Collar et al., 2019). The density ranges for these water masses show considerable overlap, which allows both diapycnal and isopycnal mixing.

Furthermore, Leadbetter et al. (2007) studied the temperature variability of the water column in the period 1981-2005 in a section at 36º N, concluding that the variability in the SAIW is consistent with changes in surface wind forcing leading to the displacement of neutral density surfaces.

Several studies have focused on the temporal variability of MOW. The analysis of hydrographic properties in the MOW core concluded that changes in MOW properties are not dominated by changes in Mediterranean Sea Water properties (Lozier and Sindlinger, 2009; Bozec et al., 2011). However, the variability of MOW is mainly dominated by year-to-year processes, some studies have described the MOW inter-annual variability as an oscillation of the water tongue shifting the dominant spreading pathway and interacting with the underlying water masses such as the North Atlantic Deep Water and LSW (Bozec et al., 2011, de Pascual-Collar, 2019).

The inter-anual variability of LSW has been described in previous works concluding that part of the variability in the water mass can be explained by diapycnal mixing with the overlying MOW (van Aken, 2000) as well as changes in the source regions over the North Atlantic basin (Leadbetter et al., 2007). Additionally, Bozec et al. (2011) studied the distribution of LSW and MOW from 1950 to 2006 observing a coupling between the spreading areas of booth water masses and the NAO index.

Since the availability of higher resolution specific regional products allows us to refine the study of OHC trends in the IBI region, the objective of the present work is to explore the spatial and temporal variability of OHC trends in the region as well as to explain its causes, providing a better understanding of the processes controlling such trends.

This paper is organized as follows: Section 2 presents the datasets used, as well as the methodology applied, to compute the OHC in the IBI region. In Sect. 3 the timeseries of OHC averaged over the whole IBI region are discussed to provide a general view of the regional trends estimated. Section 4 is devoted to show and discuss maps of trends computed in the same way that the ones provided in the GLO-OMI-trend product. Section 5 analyses the vertical profiles of OHC trends studying the variability associated with different water masses. Section 6 summarizes the availability of the data used in this article. Finally, main conclusions are summarized in Sect. 7.

2. Data and methods

Following the same methodology than in previous Copernicus Marine Ocean State Report contributions (Lima et al., 2020; Mayer et al., 2021), the estimates of OHC anomalies were computed in IBI region according to the Equation:

$$OHC = \int_{z_1}^{z_2} \rho_0 C_p \, (T_m - T_{clim}) dz \quad (1)$$

Where ρ_0 is the density at a reference depth (ρ_0=1020 kg·m^{-3}), C_p the specific heat capacity (C_p=4181.3 J·kg^{-1}·°C^{-1}), z_1 and z_2 the range of depths to compute the total OHC; T_m the monthly average potential temperature at a specific depth; and T_{clim} the climatological potential temperature of the corresponding month and depth.

https://doi.org/10.5194/sp-2022-3
Preprint. Discussion started: 23 September 2022

As can be seen in Equation (1), the OHC anomalies are obtained from integrated differences between the monthly temperature and the climatological one along a vertical profile in the ocean. In the present work the anomalies have been referenced to the monthly climatology computed between 1993 and 2019. Additionally, the OHC is presented for the typical depths of 700 m and 2000 m, but also for the upper 150 m to analyse the OHC variability in the mixing layer.

In order to allow the assessing of uncertainties of results, this study has included several data sources to provide a multi-product result, therefore all results were previously computed for a collection of data sources and combined to provide an ensemble mean and the standard deviation of the ensemble. Since the objective of this work is the analysis of OHC in the IBI region integrating results from surface down to a maximum of 2000 m depth. This study has included all Copernicus Marine products that provide gridded data of potential temperature with vertical coverage from surface down to at least 2000 m. As shown in Table 1, four different products meet these stated conditions: two model reanalysis (the global and regional ones: GLO-REA and IBI-REA, respectively) and two observations-based products (CORA and ARMOR). It is worth mentioning that when OHC were computed, the GLO-REA product did not cover the year 2020, therefore this year is considered missing for this product in the study. Similarly, some results on this work are shown below the 2000 m depth. In these cases, the corresponding data of CORA product are considered missing.

Each used product is provided in specific vertical levels with specific thickness, then all results vertically integrated were computed taking in consideration the thickness of each product level. Consequently, since most of the products used are provided with regular lat/lon grids, the surface of each grid cell depends on the latitude, thus the spatial averages of OHC (when used in this study) have been computed considering the specific surface of each product grid cell.

3. Analysis of OHC timeseries

Timeseries of OHC anomalies have been computed for all Copernicus Marine products previously defined (see Table 1) and following the methodology described in the previous section: Firstly, OHC was computed from potential temperature, then OHC anomalies were estimated, including anomalies vertically integrated (from surface down to 150 m, 700 m, and 2000 m), and finally, a last step to obtain timeseries of OHC anomalies by computing spatial averages over the whole IBI domain. Figure 1 shows combined results of all products (listed in Table 1), including in the figures the ensemble mean and the standard deviation of the product ensemble.

Attending ensemble spread, time series show an increase of uncertainties when deeper layers are included (0-700m and 0-2000m); this result can be explained by the decrease of observational data available in deeper levels. Additionally, it is remarkable the decrease of uncertainties that can be seen after 2003 in the time series integrated over the upper 2000 m. These differences in uncertainties are explained considering the remarkable improvement in the global ocean observing system achieved with the implementation of the global Argo array in 2005 (von Schuckmann et al., 2016; Abraham et al., 2013; Cheng et al., 2022; Cheng et al., 2017).

https://doi.org/10.5194/sp-2022-3
Preprint. Discussion started: 23 September 2022

Trends of time series obtained in Figure 1 show a significant warming of IBI region affecting the upper 700 m (0.4 ± 0.2 W/m^2) and 2000 m (0.5 ± 0.4 W/m^2); conversely, such a trend does not affect the mixing layer. This result suggests a dominance of the variability at intermediate-deep levels over the OHC trend. It is worth to mention that, despite the positive trends observed in the whole period (1993-2020) of time series integrated down to 700 m and 2000 m, it can be appreciated a change of trends after the year 2006. This result suggests the presence of year-to-year variations that could be affecting the long-term trends of OHC in the IBI region.

4. Analysis of regional trends of OHC

Figure 2 shows the maps of OHC trends estimated for the multi-product ensemble. To do that, the values of trend have been computed for each ensemble member. The ensemble mean and standard deviation of trends were computed for all products, however since each member is produced over a particular grid with different resolutions (see Table 1), each member was interpolated to obtain all estimations over the same grid. In this work the IBI-REA grid was used as reference for the rest of the members. Maps show the trend obtained from the ensemble mean, the uncertainty is assessed by the ensemble standard deviation. In Figure 2, the values where the uncertainty is higher than the estimated trend are masked with a transparent grey layer.

To the contrary that in Figure 1, the trends for Figure 2 were computed for the period 2005-2019. This period was selected because, as seen in the previous section, the implementation of the global Argo array produced a rise of observational data that, in the case of the OHC integrated over the upper 2000 m, implies an inhomogeneity of uncertainties in the period 2000-2005. Additionally, the period 2005-2019 is the same as the one used in GLOBAL_OMI_OHC_trend, the use of the same temporal records simplifies the comparisons between booth results. The map of trends of GLOBAL_OMI_OHC_trend product is included in Figure 2 cropping the global results to show only the IBI region. The comparison of results obtained in this work with the OMI product GLOBAL_OMI_OHC_trend (Figure 2, panels c and d), show a high level of agreement. However, it is worth mentioning the discrepancies in the intensity of negative trends off the continental slope between 48ºN and 54ºN. While in GLOBAL_OMI_OHC_trend product the negative trend is wider and less intensified, the results in this work show a more localized signal with higher intensity. Such discrepancies can be related to the increased resolution that is used in the present work.

Results of Figure 2 shows two different behaviours in the IBI region. On one hand, a negative trend that mainly affects the offshore ocean north of 38ºN. On the other hand, a tongue between 31ºN and 38ºN that shows positive values. In both cases, the observed trends (positive and negative) are subsurface intensified so the bigger is the integration depth, the bigger is the observed trend. Such intensification of trends suggests that both signals are stronger underneath the mixing layer, therefore they are more related to the evolution of intermediate and deep water masses than to the year-to-year interaction with the atmosphere. The warming of the region around 34ºN (see Figure 2c) suggests that the MOW water mass may be involved on this trend, this hypothesis is consistent with de Pascual-Collar et al. (2019) that described the region comprised around the

https://doi.org/10.5194/sp-2022-3
Preprint. Discussion started: 23 September 2022

Horseshoe basin (bounded by the parallels 35ºN and 37ºN and meridians 14ºW and 12ºW) as highly sensitive to the advancement/retreat of MOW. This hypothesis is examined in the following section.

5. Analysis of OHC trends across different water masses

For a deeper analysis of the OHC trends, it was analysed the vertical profile of the trends derived from the IBI-REA product averaged over three different study subregions (see geographical coverages in Figure 3a). The IBI-REA product was selected as the reference product for this purpose because it assimilates observational (in situ and satellite) data and uses the GLO-REA product as initial and boundary conditions. The comparison of the trends map of IBI-REA (Figure 3a) with the ensemble mean trend map (Figure 2c) reveals a high resemblance between both results. The more relevant differences correspond to the region of positive trends at 43ºN: whereas the ensemble mean results in positive, but not significant, trends, in the case of the IBI-REA, the region comprises significant positive trends.

The analysis of trend profiles is done over the three boxes marked on Figure 3a, these boxes have been selected to represent the two positive/negative behaviours of trends (regions located at 34ºN and 49ºN respectively) seen in the previous section, and a third box to explore the positive trends at 43ºN. Hereafter these boxes will be referred as subregions 34N, 49N, and 43N respectively. The trends of OHC averaged on the three boxes has been computed at each level to obtain a vertical profile of trends. These trend profiles have been presented in Figure 3 (panels b, c, and d) combined with the temperature and salinity data on a yearly basis. The different markers used correspond to the different trends observed for each depth. Therefore, the θ/S diagrams shown allows to discuss the trends of OHC at each layer linking these results with the different water masses observed in the region.

The three θ/S profiles shown in Figure 3 are consistent with the water masses that the literature has described in the north-eastern Atlantic: The SAIW characterized by a salinity minima at potential density σ_θ=27.2 kg/m^3, the salinity maxima connected with MOW at the neutral density surface σ_θ=27.6 kg/m^3, and a deeper salinity minima corresponding to LSW underneath the isopycnal σ_θ=27.8 kg/m^3 (Talley and McCarney, 1982; Iorga and Lozier, 1999(a); Iorga and Lozier, 1999(b); van Aken, 2000; Prieto et al., 2013; de Pascual-Collar et al., 2019).

Results in Figure 3 show a cooling trend in the upper subsurface levels corresponding to SAIW. These trends are consistent with changes in thermocline thickness forced by temporal changes in Ekman pumping described in Leadbetter et al. (2007).

The levels associated with MOW show a cooling in the subregion 49N, while subregions 34N and 43N show a positive trend of OHC. Additionally, results show that the variability of temperature and salinity are correlated (the markers at each level are aligned), thus the positive trend of temperature entails a positive trend of salinity. These results suggest that the MOW variability observed in 34N and 43N can be caused by a displacement of the water mass boundaries towards the west (so the region becomes warmer and saltier). This result is consistent with Pascual-Collar et al. (2019) that described a displacement of the MOW boundaries towards the west in the Horseshoe basin in the period 2006-2017. Conversely, the cooling and freshening trends observed in subregion 49N suggests a retreat of MOW towards the south. This result is consistent with

https://doi.org/10.5194/sp-2022-3
Preprint. Discussion started: 23 September 2022

studies that observed a significant anti-correlation between the western and northern boundary transports of MOW, thus the anomalies at the continental slope of Gulf of Biscay are out of phase with anomalies along the westward pathway in the subtropical gyre (Bozec et al., 2011). The warming of the westward limits of the MOW waters (boxes 34N and 43N) and the cooling of the northward boundary of MOW (subregion 49N) in the period 2005-2020 leads to the conclusion that in this period the MOW tongue moved westward, retracting from its northern limit.

Regarding deeper water levels, Figure 3 shows the positive trends in the levels corresponding to the LSW in the three study subregions; this result can be explained by the connection between of MOW and LSW in the region (Bozec et al., 2011; Pascual-Collar, 2019). This warming in upper layers of the LSW layer observed leads to conclude that the retreat towards the west of the LSW in the period 2005-2020 can entail advances of warmer water masses from the east, producing positive OHC trends in isopicnals below σ_θ=27.8 kg/m^3.

6. Data availability

All data used in this article can be downloaded from the Copernicus Marine Environment Monitoring Service (2022) web page. The description of the data products as well as their names, spatial and temporal coverages, and documentation, are summarized in Table 1.

7. Conclusions

The present work states the key role that subsurface water masses play in the OHC trends in the IBI region. OHC OMIs are computed as integrated values between the surface down to a specific depth. Being these indicators useful to evaluate the total heat content stored in a region. Specifically, in the period 1993-2020, the IBI region suffered a warming of +0.3 W/m^2 and +0.4 W/m^2 in the upper 700 m and 2000 m, respectively. Despite of the regional analysis of trends of OHC integrated in different depths may provide some clues about the origin of trends, a finer analysis of the different water masses involved concludes that integrated trend is the result of different trends (positive and negative) observed in different layers. In the IBI region, on the period 2005-2020 three water masses (SAIW, MOW and LSW) have shown significant trends of OHC, Table 2 summarises the averaged thermic trends observed in each study subregion for each density layer associated to each water type. The SAIW found in the upper levels behind the mixing layer, has shown a negative trend that affects the three boxes studied. According to our results, the cooling of this water mass ranges from -0.1 W/m^3 in the southernmost region (34N) up to -0.7 W/m^3 in the box 49N (See Table 2). These results can be explained by changes in wind forcing associated with the North Atlantic Oscillation (Leadbetter et al., 2007). Since the study has not found trends in the mixing layer, it can be conjectured that this process is responsible for the surface conditions affecting the OHC all over the IBI region.

The intermediate depths of the IBI domain are mainly dominated by MOW, this water mass shows trends of OHC associated with the boundaries of the water tongue, therefore we conclude that those trends are related with the inter-annual variability of

https://doi.org/10.5194/sp-2022-3
Preprint. Discussion started: 23 September 2022

the boundaries of this water mass. The results here presented demonstrates that, between 2005 and 2019, MOW tongue shows a trend of -0.9 W/m^3 in its northern boundary (box 49N) and a warming trend of +0.3 W/m^3 in the boxes at the western boundary (34N and 43N); these trends are correlated to proportional trends in salinity, suggesting a displacement of the MOW tongue from the north to the west in the period.

The deeper water mass studied in this work corresponds to the LSW, our results have shown that between 2005 and 2020 the LSW was displaced towards the west allowing the advance towards the east of warmer water masses, such displacement entails a thermic warming of the region of +0.2 W/m^3 in 34N and +0.3 W/m^3 in 43N and 49N.

As far as detected within the limited temporal extension of the products used (27 years), both analysis of trends, the one from integrated time series (Figure 1) and the one made for water masses (Figure 3), show trends associated with an inter-annual variability that alternates periods of warming and cooling conditions. Therefore, the present study did not find long-term trends associated with changes in properties of the source water masses, but with the displacement of such water masses. Since the IBI domain hosts the core of the MOW water mass, this long-term analysis can be pursued in a future work.

Acknowledgements

The authors thank to Copernicus Marine Environment Monitoring Service for providing the data for the article. Additionally, the helpful comments of Karina von Schuckmann and the other referees are gratefully acknowledged.

References

Abraham, J. P., Baringer, M., Bindoff, N. L., Boyer, T., Cheng, L. J., Church, J. A., Conroy, J. L., Domingues, C. M., Fasullo, J. T., Gilson, J., Goni, G., Good, S. A., Gorman, J. M., Gouretski, V., Ishii, M., Johnson, G. C., Kizu, S., Lyman, J. M., Macdonald, A. M., Minkowycz, W. J., Moffitt, S. E., Palmer, M. D., Piola, A. R., Reseghetti, F., Schuckmann, K., Trenberth, K. E., Velicogna, I., and Willis, J. K.: A review of global ocean temperature observations: Implications for ocean heat content estimates and climate change. Reviews of Geophysics, 51(3), 450-483, 2013.

Bozec, A., Lozier, M. S., Chasignet, E. P., and Halliwel, G. R.: On the variability of the Mediterranean Outflow Water in the North Atlantic from 1948 to 2006, J. Geophys. Res.-Oceans, 116, C09033, doi:10.1029/2011JC007191, 2011.

Cheng, L., K. E. Trenberth, J. Fasullo, T. Boyer, J. Abraham, and J. Zhu, 2017: Improved estimates of ocean heat content from 1960–2015. Sci. Adv., 3, e1601545, doi:10.1126/sciadv.1601545, 2017.

Cheng, L., Foster, G., Hausfather, Z., Trenberth, K. E., and Abraham, J.: Improved quantification of the rate of ocean warming. Journal of Climate, 1-37, doi:10.1175/JCLI-D-21-0895.1, 2022.

https://doi.org/10.5194/sp-2022-3
Preprint. Discussion started: 23 September 2022

de Pascual-Collar, Á., García-Sotillo, M., Levier, B., Aznar, R., Lorente, P., Amo-Baladrón, A., and Álvarez-Fanjul, E.: Regional circulation patterns of Mediterranean Outflow Water near the Iberian and African continental slopes. Ocean Science, 15(3), 565-582, doi: https://doi.org/10.5194/os-15-565-2019, 2019.

Gulev, S. K., Thorne, P. W., Ahn, J., Dentener, F. J., Domingues, C.M., Gerland, S., Gong, D., Kaufman, D. S., Nnamchi, H. C., Quaas, J., Rivera, J. A., Sathyendranath, S., Smith, S. L., Trewin, B., von Schuckmann, K., and Vose, R. S.: Changing State of the Climate System. In Climate Change 2021: The Physical Science Basis. Contribution of Working Group I to the Sixth Assessment Report of the Intergovernmental Panel on Climate Change [Masson Delmotte, V., Zhai, P., Pirani, A., Connors, S. L., Péan, C., Berger, S., Caud, N., Chen, Y., Goldfarb, L., Gomis, M. I., Huang, M., Leitzell, K., Lonnoy, E., Matthews, J. B. R., Maycock, T. K., Waterfield, T., Yelekçi, O., Yu, R., and Zhou, B. (eds.)]. Cambridge University Press, Cambridge, United Kingdom and New York, NY, USA, pp. 287–422, doi:10.1017/9781009157896.004, 2021.

Iorga, M. C. and Lozier, M. S.: Signatures of the Mediterranean outflow from a North Atlantic climatology 1. Salinity and density fields, J. Geophys. Res., 104, 25985–26009, 1999a.

Iorga, M. C. and Lozier, M. S.: Signatures of the Mediterranean outflow from a North Atlantic climatology 2. Diagnostic velocity fields, J. Geophys. Res., 104, 26011–26029, 1999b

Leadbetter, S. J., Williams, R. G., McDonagh, E. L., and King, B. A.: A twenty year reversal in water mass trends in the subtropical North Atlantic, Geophys. Res. Lett., 34, 1–6, doi:10.1029/2007GL029957, 2007.

Levitus, S., Antonov, J., and Boyer, T.: Warming of the world ocean, 1955–2003. Geophysical research letters, 32(2), doi:10.1029/2004GL021592, 2005.

Levitus, S., Antonov, J. I., Boyer, T. P., Baranova, O. K., Garcia, H. E., Locarnini, R. A., Mishonov, A. V., Reagan, J. R., Seidov, D., Yarosh, E. S., and Zweng, M. M.: World ocean heat content and thermosteric sea level change (0–2000 m), 1955–2010. Geophysical Research Letters, 39(10), doi:10.1029/2012GL051106, 2012.

Lima L., Peneva E., Ciliberti E., Masina S., Lemieux B., Storto A., Chtirkova B. (2020) Ocean heat content in the Black Sea. In: von Schuckmann, K., Le Traon, P. Y., Smith, N., Pascual, A., Djavidnia, S., Gattuso, J. P., Grégoire, M., Nolan, G., Aaboe, S., Álvarez-Fanjul, E., Aouf, L., Aznar, R., Badewien, T. H., Behrens, A., Berta, M., Bertino, L., Blackford, J., Bolzon, G., Borile, F., Bretagnon, M., Brewin, R. J. W., Canu, D., Cessi, P., Ciavatta, S., Chapron, B., Trang Chau, T. T., Chevallier, F., Chtirkova, B., Ciliberti, S., Clark, J. R., Clementi E., Combot, C., Comerma, E., Conchon, A., Coppini, G., Corgnati, L., Cossarini, G., Cravatte, S., de Alfonso, M., de Boyer Montégut, C., De Lera Fernández, C., de los Santos, F. J., Denvil-

https://doi.org/10.5194/sp-2022-3
Preprint. Discussion started: 23 September 2022

Sommer, A., de Pascual-Collar, A., Dias Nunes, P. A. L., Di Biagio, V., Drudi, M., Embury, O., Falco, P., Fanton d'Andon, O., Ferrer, L., Ford, D., Freund, H., García León, M., García-Sotillo. M. , García-Valdecasas, J. M., Garnesson, P., Garric, G., Gasparin, F., Gehlen, M., Genua-Olmedo, A., Geyer, G., Ghermandi, A., Good, S. A., Gourrion, J., Greiner, E., Griffa, A., González, M., Hernández-Carrasco, I., Isoard, E., Kenned, J. J., Kay. S., Korosov, A., Laanemäe, K., Land, P. E., Lavergne, T., Lazzari, P., Legeais, JF., Lemieux, B., Levier, B., Llovel, W., Lyubartsev, V., Le Traon, PY., Lien, V. S., Lima, L., Lorente, P., Mader, J., Magaldi, M. G., Maljutenko, I., Mangin, A., Mantovani, C., Marinova, V., Masina, S., Mauri, E., Meyerjürgens, J., Mignot, A., McEwan, R., Mejia, C., Melet, A., Menna, M., Meyssignac, B., Mouche, A., Mourre, B., Müller, M., Notarstefano, G., Orfila, A., Pardo, S., Peneva, E., Pérez-Gómez, B., Perruche, C., Peterlin, M., Poulain, PM., Pinardi, N., Quilfen, Y., Raudsepp, U., Renshaw, R., Révelard, A., Reyes-Reyes, E., Ricker, M., Rodríguez-Rubio, P., Rotllán, P., Royo Gelabert, E., Rubio, A., Ruiz-Parrado, I., Sathyendranath, S., She, J., von Schuckmann, K., Solidoro, C., Stanev, E.V., Staneva, J., Storto, A., Su, J., Tajalli Bakhsh, T., Tilstone, G. H., Tintoré, J., Toledano, C., Tournadre, J., Tranchant, B., Uiboupin, R., Valcarcel, A., Valcheva, N., Verbrugge, N., Vrac, M., Wolff, JO., Zambianchi, E., Zielinski, O., Zinck, AS., and Zunino, S.: Copernicus marine service ocean state report, issue 4. Journal of Operational Oceanography, 13(sup1), S1-S172, doi:10.1080/1755876X.2020.1785097, 2020.

Lozier, M. S., and Sindlinger, L.: On the Source of Mediterranean OverflowWater Property Changes, J. Phys. Oceanogr., 39, 1800– 1817, doi:10.1175/2009JPO4109.1, 2009.

Michael Mayer, Vidar S. Lien, Kjell Arne Mork, Karina von Schuckmann, Maeva Monier, Eric Greiner: Ocean heat content in the High North. In:

von Schuckmann, K., Le Traon, PY., Smith, N., Pascual, A., Djavidnia, S., Gattuso, JP., Grégoire, M., Aaboe, S., Alari, V., Alexander, B. E., Alonso-Martirena, A., Aydogdu, A., Azzopardi, J., Bajo, M., Barbariol, F., Batistić, M., Behrens, A., Ben Ismail, S., Benetazzo, A., Bitetto, I., Borghini, M., Bray, L., Capet, A., Carlucci, R., Chatterjee, S., Chiggiato, J, Ciliberti, S., Cipriano, G., Clementi, E., Cochrane, P., Cossarini, G., D'Andrea, L, Davison, S., Down, E., Drago, A., Druon, JN., Engelhard, G., Federico, I., Garić, R., Gauci, A., Gerin, R., Geyer, G., Giesen, R., Good, S., Graham, R., Grégoire, M., Greiner, E., Gundersen, K., Hélaouët, P., Hendricks, S., Heymans, J. J., Holt, J., Hure, M., Juza, M., Kassis, D., Kellett, P., Knol-Kauffman, M., Kountouris, P., Kõuts, M., Lagemaa, P., Lavergne, T., Legeais, JF., Le Traon, PY., Libralato, S., Lien, V. S., Lima, L., Lind, S., Liu, Y., Macías, D., Maljutenko, I., Mangin, A., Männik, A., Marinova, V., Martellucci, R., Masnadi, F., Mauri, E., Mayer, M., Menna, M., Meulders, C., Møgster, J. S., Monier, M., Arne Mork, K., Müller, M., Øie Nilsen, J. E., Notarstefano, G., Oviedo, J. L., Palerme, C., Palialexis, A., Panzeri, D., Pardo, S., Peneva, E., Pezzutto, P., Pirro, A., Platt, T., Poulain, PM., Prieto, L., Querin, S., Rabenstein, L., Raj, R. P., Raudsepp, U., Reale, M., Renshaw, R., Ricchi, A., Ricker, R., Rikka, S., Ruiz, J., Russo, T., Sanchez, J., Santoleri, R., Sathyendranath, S., Scarcella, G., Schroeder, K., Sparnocchia,S., Spedicato, M. T., Stanev, E., Staneva, J., Stocker, A., Stoffelen, A., Teruzzi, A., Townhill, B., Uiboupin, R., Valcheva, N., Vandenbulcke, L.,

https://doi.org/10.5194/sp-2022-3
Preprint. Discussion started: 23 September 2022

Vindenes, H., von Schuckmann, K., Vrgoč, N., Wakelin, S., and Zupa, W.: Copernicus Marine Service Ocean State Report, Issue 5, Journal of Operational Oceanography, 14:sup1, 1-185, doi:10.1080/1755876X.2021.1946240, 2021.

Potter, R. A., and Lozier, M. S.: On the warming and salinification of the Mediterranean outflow waters in the North Atlantic, Geophys. Res. Lett., 31, 1–4, doi:10.1029/2003GL018161, 2004.

Prieto, E., González-Pola, C., Lavín, A., Sánchez, R. F., and Ruiz- Villarreal, M.: Seasonality of intermediate waters hydrography west of the Iberian Peninsula from an 8 yr semiannual time series of an oceanographic section, Ocean Sci., 9, 411–429, doi:10.5194/os-9-411-2013, 2013.

Talley, L. D., and McCartney, M. S.: Distribution and Circulation of Labrador Sea Water, J. Phys. Oceanogr., 12, 1189–1205, doi:10.1175/1520-0485(1982)012<1189:DACOLS>2.0.CO;2, 1982.

Trenberth, K. E., Fasullo, J. T., and Balmaseda, M.: Earth's energy imbalance. J. Climate, 27, 3129–3144, doi:10.1175/JCLI-D-13-00294.1, 2014.

van Aken, H. M.: The hydrography of the mid-latitude North- east Atlantic Ocean II: The intermediate water masses, Deep-Sea Res., 47, 789–824, doi:https://doi.org/10.1016/S0967-0637(99)00112-0, 2000.

von Schuckmann, K., Balmaseda, M., and Simoncelli, S.: Ocean Heat Content. In: von Schuckmann, K. Le Traon, PY., Alvarez-Fanjul, E., Axell, L., Balmaseda, M., Breivik, LA., Brewin, R. J. W., Bricaud, C., Drevillon, M., Drillet, Y., Dubois, C., Embury, O., Etienne, H., García-Sotillo, M., Garric, G., Gasparin, F., Gutknecht, E., Guinehut, S., Hernandez, F., Juza, M., Karlson, B., Korres, G., Legeais, JF., Levier, B., Lien, V. S., Morrow, R., Notarstefano, G., Parent, L., Pascual-Collar, A., Pérez-Gómez, B., Perruche, C., Pinardi, N., Pisano, A., Poulain, PM., Pujol, I. M., Raj, R. P., Raudsepp, U., Roquet, H., Samuelsen, A., Sathyendranath, S., She, J., Simoncelli, S., Solidoro, C., Tinker, J., Tintoré, J., Viktorsson, J., Ablain, M., Almroth-Rosell, E., Bonaduce, A., Clementi, E., Cossarini, G., Dagneaux, Q., Desportes, C., Dye, S., Fratianni, C., Good, S., Greiner, E., Gourrion, J., Hamon, M., Holt, J., Hyder, P, Kennedy, J., Manzano-Muñoz, F., Melet, A, Meyssignac, B., Mulet, S., Buongiorno Nardelli, B., O'Dea, E., Olason, E., Paulmier, A., Pérez-González, I., Reid, R., Racault, MF., Raitsos, D. E., Ramos, A., Sykes, P., Szekely T., and Verbrugge, N.: The Copernicus Marine Environment Monitoring Service Ocean State Report, Journal of Operational Oceanography, Volume 9 - Issue sup2: The Copernicus Marine Environment Monitoring Service Ocean, doi:10.1080/1755876X.2016.1273446, 2016.

von Schuckmann, K., Storto, A., Simoncelli, S., Raj, R. P., Samuelsen, A., Pascual-Collar, A., Garcia-Sotillo, M., Szerkely, T.: Ocean Heat Content. In: von Schuckmann, K., Le Traon, PY., Smith, N., Pascual, A., Brasseur, P., Fennel, K., Djavidnia,

https://doi.org/10.5194/sp-2022-3
Preprint. Discussion started: 23 September 2022

S., Aaboe, S., Fanjul, E. A., Autret, E., Axell, L., Aznar, R., Benincasa, M., Bentamy, A., Boberg, F., Bourdallé-Badie, R., Nardelli, B. B., Brando, V. E., Bricaud, C., Breivik, LA., Brewin, R. J. W., Capet, A., Ceschin, A., Ciliberti, S., Cossarini, G., de Alfonso, M., Pascual-Collar, A., de Kloe, J., Deshayes, J., Desportes, C., Drévillon, M., Drillet, Y., Droghei, R., Dubois, C., Embury, O., Etienne, E., Fratianni, C., García Lafuente, J. , Garcia-Sotillo, M., Garric, G., Gasparin, F., Gerin, R., Good, S., Gourrion, J, Grégoire, M., Greiner, E, Guinehut, S., Gutknecht, E., Hernandez, F., Hernandez, O., Høyer, J., Jackson, L., Jandt, S., Josey, S., Juza, M., Kennedy, J., Kokkini, Z., Korres, G., Kõuts, M., Lagemaa, P., Lavergne, T., le Cann, B., Legeais, JF., Lemieux-Dudon, B., Levier, B., Lien, V., Maljutenko, I., Manzano, F., Marcos, M., Marinova, V., Masina, S., Mauri, E., Mayer, M., Melet, A., Mélin, F., Meyssignac, B., Monier, M., Müller, M., Mulet, S., Naranjo, C., Notarstefano, G., Paulmier, A., Pérez Gomez, B., Pérez Gonzalez, I., Peneva, E., Perruche, C., Peterson, K. A., Pinardi, N., Pisano, A., Pardo, S., Poulain, PM., Raj, R. P., Raudsepp, U., Ravdas, M., Reid, R., Rio, MH., Salon, S., Samuelsen, A., Sammartino, M., Sammartino, S., Britt Sandø, A., Santoleri, R., Sathyendranath, S., She, J., Simoncelli, S., Solidoro, C., Stoffelen, A., Storto, A., Szerkely, T., Tamm, S., Tietsche, S., Tinker, J., Tintore, J., Trindade, A., van Zanten, D. , Vandenbulcke, L., Verhoef, A., Verbrugge, N., Viktorsson, L., Wakelin, S. L., Zacharioudaki, A., and Zuo, H.: Copernicus Marine Service Ocean State Report. Journal of Operational Oceanography, 11(sup1), S1–S142, doi:10.1080/1755876X.2018.1489208, 2018.

von Schuckmann, K., Cheng, L., Palmer, M. D., Hansen, J., Tassone, C., Aich, V., Adusumilli, S., Beltrami, H., Boyer, T., Cuesta-Valero, F. J., Desbruyères, D., Domingues, C., García-García, A., Gentine, P., Gilson, J., Gorfer, M., Haimberger, L., Ishii, M., Johnson, G. C., Killick, R., King, B. A., Kirchengast, G., Kolodziejczyk, N., Lyman, J., Marzeion, B., Mayer, M., Monier, M., Monselesan, D. P., Purkey, S., Roemmich, D., Schweiger, A., Seneviratne, S. I., Shepherd, A., Slater, D. A., Steiner, A. K., Straneo, F., Timmermans, M., and Wijffels, S. E.: Heat stored in the Earth system: Where does the energy go? Earth Syst. Sci. Data, 12, 2013–2041, doi:10.5194/essd-12-2013-2020, 2020.

WMO: World Meterological Organisation Bulletin, 66(2), https://public.wmo.int/en/resources/bulletin, 2017.

https://doi.org/10.5194/sp-2022-3
Preprint. Discussion started: 23 September 2022

IBI-REA	**Copernicus product ID:** IBI_MULTIYEAR_PHY_005_003		
Type: Model reanalysis	**Resolution:** 0.083° x 0.083°	**Temporal Coverage:** 1993-2020	**Vertical Coverage:** 0 - 5500m (50 levels)
• **PUM:** https://catalogue.marine.copernicus.eu/documents/PUM/CMEMS-IBI-PUM-005-003.pdf • **QUID:** https://catalogue.marine.copernicus.eu/documents/QUID/CMEMS-IBI-QUID-005-003.pdf			
GLO-REA	**Copernicus product ID:** GLOBAL_MULTIYEAR_PHY_001_030		
Type: Model reanalysis	**Resolution:** 0.083° x 0.083°	**Temporal Coverage:** 1993-2019	**Vertical Coverage:** 0-5500m (50 levels)
• **PUM:** https://catalogue.marine.copernicus.eu/documents/PUM/CMEMS-GLO-PUM-001-030.pdf • **QUID:** https://catalogue.marine.copernicus.eu/documents/QUID/CMEMS-GLO-QUID-001-030.pdf			
CORA	**Copernicus product ID:** INSITU_GLO_TS_OA_REP_OBSERVATIONS_013_002_b		
Type: In situ obs.	**Resolution:** ~0.36° x 0.5°	**Temporal Coverage:** 1993-2020	**Vertical Coverage:** 0–2000m (152 levels)
• **PUM:** https://catalogue.marine.copernicus.eu/documents/PUM/CMEMS-INS-PUM-013-002-ab.pdf • **QUID:** https://catalogue.marine.copernicus.eu/documents/QUID/CMEMS-INS-QUID-013-002b.pdf			
ARMOR	**Copernicus product ID:** MULTIOBS_GLO_PHY_TSUV_3D_MYNRT_015_012		
Type: In situ + sat. obs.	**Resolution:** 0.25° x 0.25°	**Temporal Coverage:** 1993-2020	**Vertical Coverage:** 0–5500m (50 levels)
• **PUM:** https://catalogue.marine.copernicus.eu/documents/PUM/CMEMS-MOB-PUM-015-012.pdf • **QUID:** https://catalogue.marine.copernicus.eu/documents/QUID/CMEMS-MOB-QUID-015-012.pdf			
GLO-OMI-trend	**Copernicus product ID:** GLOBAL_OMI_OHC_trend		
Type: OMI	**Resolution:** 0.25° x 0.25°	**Temporal Coverage:** 2005-2009	**Vertical Coverage:** Integrated 0-2000 (1 level)
• **PUM:** https://catalogue.marine.copernicus.eu/documents/PUM/CMEMS-OMI-PUM-GLO-OHC.pdf • **QUID:** https://catalogue.marine.copernicus.eu/documents/QUID/CMEMS-OMI-QUID-GLO-OHC.pdf			

Table 1: List of Copernicus Marine products used for the computation of Ocean Heat Content (OHC) in Iberia-Biscay-Ireland region (IBI).

https://doi.org/10.5194/sp-2022-3
Preprint. Discussion started: 23 September 2022

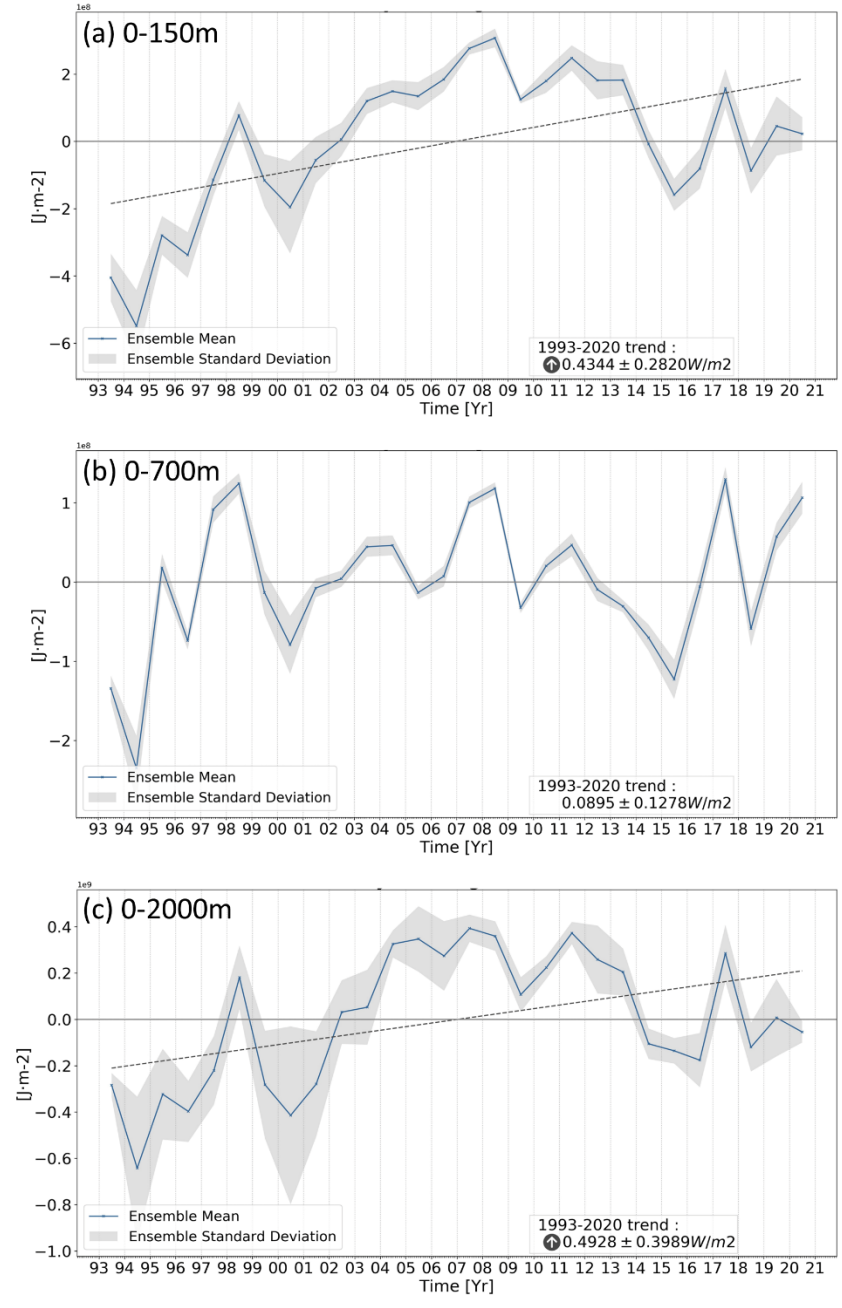

Figure 1: OHC averaged in the IBI domain integrated from the ocean's surface down to 150 m (a), 700 m (b), and 2000 m (c), respectively. Timeseries computed from 4 Copernicus Marine products (i.e.: IBI-REA, GLO-REA, CORA, and ARMOR), providing a multi-product approach. Blue line represents the ensemble mean and shaded grey areas represent the standard deviation of the ensemble. The analysis of trends (at 95% confidence interval) computed in the period 1993-2020 is included (bottom-right box). Trend lines (dashed line) are only included in the figures when a significant trend is obtained.

https://doi.org/10.5194/sp-2022-3
Preprint. Discussion started: 23 September 2022

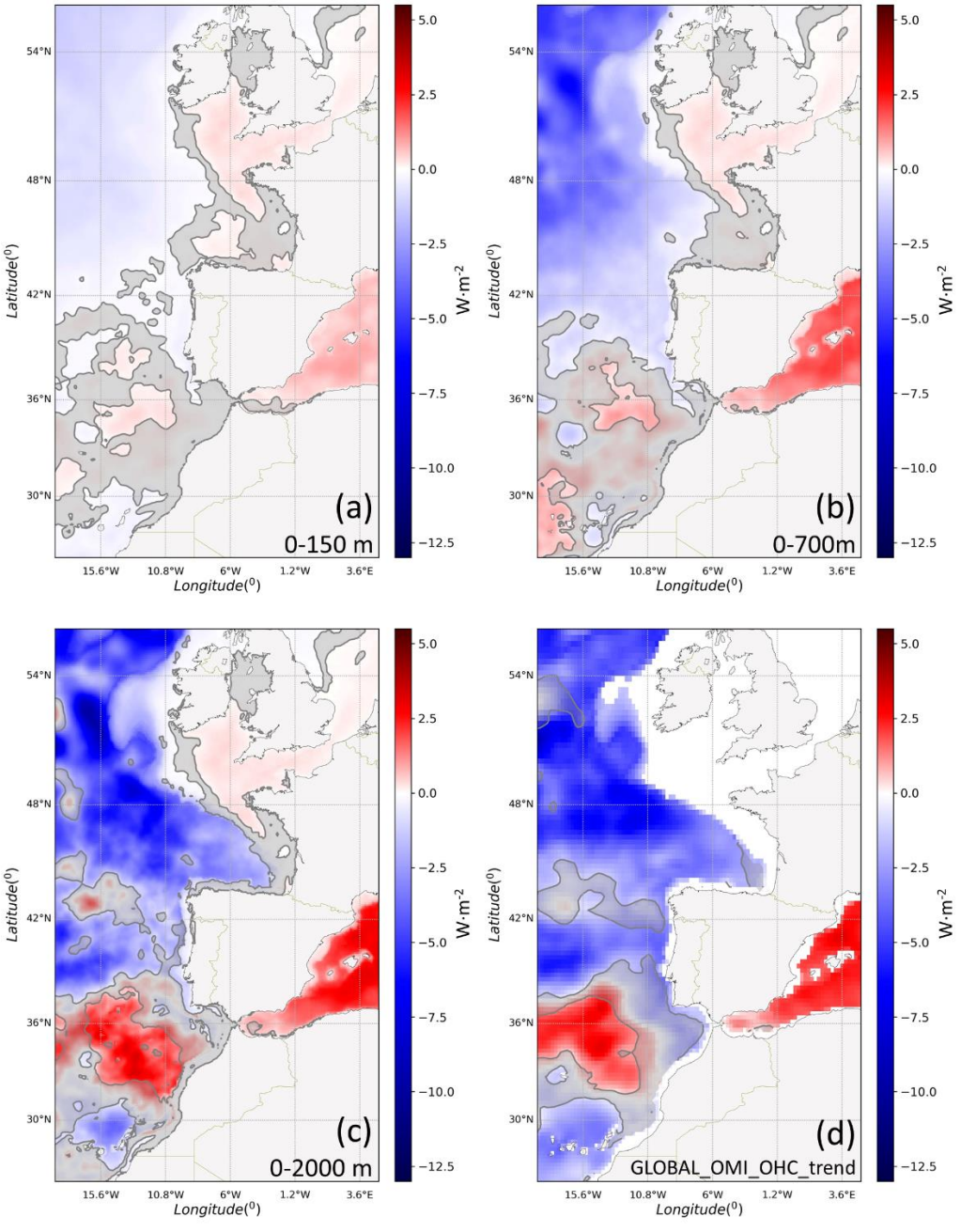

Figure 2: Maps of regional OHC trend over the period 2005-2019 at 0-150 m (a), 0-700 m (b), and 0-2000 m (c). Trends computed using the 4 Copernicus Marine products (IBI-REA, GLO-REA, CORA, and ARMOR) providing a multi-product approach. Shaded colours represent mean trends (using all products), while shaded grey indicates areas with less robust signatures (where the noise (ensemble standard deviation of trends) exceeds the signal (ensemble mean))). (d) same as panel c but obtained from GLO-OMI-trend.

https://doi.org/10.5194/sp-2022-3
Preprint. Discussion started: 23 September 2022

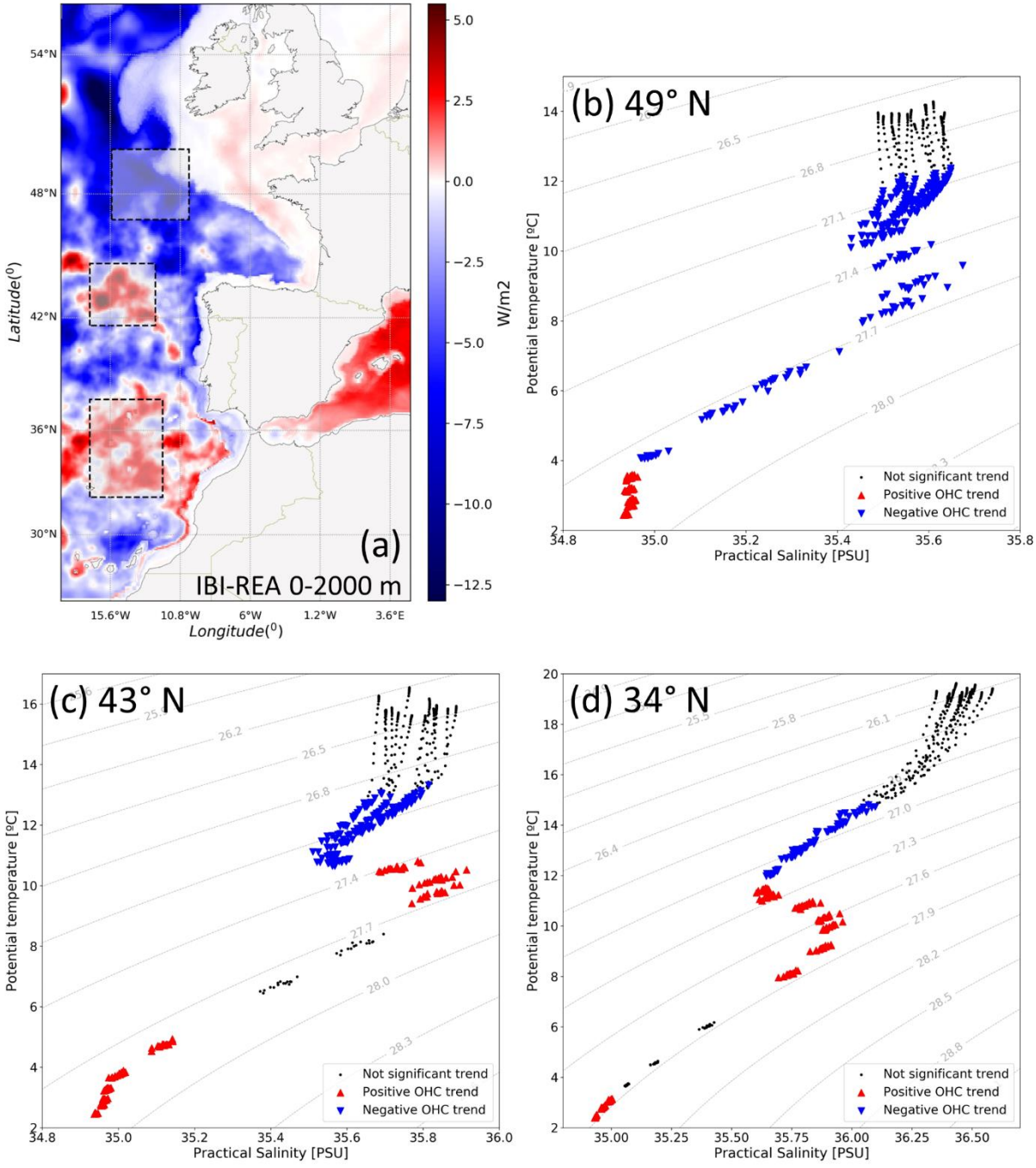

Figure 3: (a) Map of regional ocean heat content over the period 2005-2019 (0-2000 m) derived from the IBI-REA product. Dashed rectangles denote the regions where θ/S diagrams are averaged. (b, c, and d) Averaged θ/S diagrams in the subregions at 49ºN (b), 43ºN (c), and 34ºN (d), respectively. Markers have been divided depending on the significance of trend computed from OHC at each level: Triangles denote significant positive/negative (upward red/downward blue) OHC trends and dots represent levels where OHC trends are not significant. Gray isolines show the field of potential density anomaly referenced to the sea surface (σ_θ in kg·m^{-3}).

https://doi.org/10.5194/sp-2022-3
Preprint. Discussion started: 23 September 2022

Water type	Averaged Trend [W/m^3] at IBI Subregions		
	34N	43N	49N
Sub-Artic Intermediate Water (SAIW)	-0.1	-0.2	-0.7
Mediterranean Outflow Water (MOW)	+0.3	+0.3	-0.9
Labrador Sea Water (LSW)	+0.2	+0.3	+0.3

Table 2: Mean thermic trends (in W/m^3) of the different water masses identified in the IBI subregions (34N, 43N, and 49N), see spatial domains in Figure 3a.

405